Preprint typeset using LaTeX style emulateapj v. 2/19/04

EFFECTS OF COSMIC INFRARED BACKGROUND ON
HIGH ENERGY DELAYED GAMMA-RAYS FROM GAMMA-RAY BURSTS

Kohta Murase[1], Katsuaki Asano[2], Shigehiro Nagataki[1,3]

ABSTRACT

Regenerated high energy emissions from gamma-ray bursts (GRBs) are studied in detail. If the primary emission spectrum extends to TeV range, these very high energy photons will be absorbed by the cosmic infrared background (CIB). The created high energy electron-positron pairs up-scatter not only cosmic microwave background (CMB) photons but also CIB photons, and secondary photons are generated in the GeV-TeV range. These secondary delayed photons may be observed in the near future, and useful for a consistency check for the primary spectra and GRB physical parameters. The up-scattered CIB photons cannot be neglected for low redshift bursts and/or GRBs with a relatively low maximum photon energy. The secondary gamma-rays also give us additional information on the CIB, which is uncertain in observations so far.

Subject headings: gamma rays: bursts — infrared: general — radiation mechanisms: non-thermal

1. INTRODUCTION

Gamma-ray bursts (GRBs) are highly relativistic astrophysical objects located at a cosmological distance. The gamma-ray emissions with highly nonthermal spectra lead to the relativistic shock scenario (see reviews, e.g., (Mészáros 2006; Zhang 2007)). The internal shock model is one of widely accepted models. In this model, the GRB prompt emission is explained by synchrotron radiation from relativistic electrons accelerated in shocks generated by collisions among the subshells, although the mechanism of prompt emission is not fully understood. Theoretically, several emission mechanisms of GeV-TeV emission have been proposed. The synchrotron self-inverse Compton mechanism (SSC) is one of them (Papathanassiou & Mészáros 1996; Dai & Lu 2002b; Guetta & Granot 2003; Peer & Waxman 2004; Casanova et al. 2006). While this belongs to the leptonic scenarios, there are hadronic scenarios. In GRBs, protons can be accelerated up to the ultra high energy region. If this is possible, high energy protons can interact with gamma-rays and produce not only electron-positron pairs but also pions and muons that decay into neutrinos, electons, positrons, and gamma-rays (Waxman & Bahcall 1997; Asano 2005; Asano & Takahara 2003). Sufficiently high energy protons can emit gamma-rays by synchrotron radiation (Totani 1998). Synchrotron radiation by electrons, positrons and muons produced via photomeson production and photopair production can also contribute to resulting spectra (Dermer & Atoyan 2004; Asano & Inoue 2007). Neutrino detection is strong evidence of baryon acceleration and expected by future neutrino detectors such as IceCube (Waxman & Bahcall 1997; Guetta et al. 2001; Guetta et al. 2004a; Dermer and Atoyan 2003; Murase & Nagataki 2006a; Asano & Nagataki 2006).

Sufficiently high energy photons, including photons originating from protons, make pairs mainly via $\gamma\gamma \rightarrow e^+e^-$ interaction in the subshells and cannot escape from the source due to the large optical depth, which depends on the bulk Lorentz factor (Lithwick & Sari 2001; Razzaque et al. 2004). Even if such high energy photons escape from the sub-shells, these photons may suffer from interactions with the cosmic infrared background (CIB) and, especially, largely be absorbed for high-z GRBs such as $z \gtrsim 1$. Hence, the detection of TeV photons will be very difficult, unless the GRB location is nearby. The secondary electron-positron pairs generated by attenuation are very energetic, so that they scatter on numerous cosmic microwave background (CMB) photons by the inverse-Compton (IC) process. Such secondary photons will be observed as delayed GeV emissions (Cheng & Cheng 1996; Dai & Lu 2002b; Guetta & Granot 2003; Razzaque et al. 2004; Casanova et al. 2006). The secondary delayed emission is an indirect evidence of the intrinsic TeV emission as well as a clue to probing the intergalactic magnetic (IGM) field, which is poorly known (Plaga 1995). Such delayed emission has been discussed in terms of not only the internal shock model but also the external shock model (Mészáros & Rees 1994; Mészáros et al. 1994; Dermer et al. 2000; Zhang & Mészáros 2001; Derishev et al. 2002; Wang et al. 2001b; Wang et al. 2004; Ando 2004). They could be distinguishable by the distinct spectral evolution behavior.

The photon attenuation due to the CIB is very useful as an indirect probe of the CIB radiation field, which is not fully understood. The direct observation of the CIB is difficult, because of the bright foreground emission associated with zodiacal light as well as emission from our Galaxy. COBE DIRBE and COBE FIRAS have succeeded in highly significant detections of a residual diffuse infrared background, providing an upper bound on the CIB in the infrared regime. Lower limits from galaxy counts help in determining the spectral energy distribution (SED) of the CIB at wavelengths, where no COBE data is available. Despite the dramatic progress in observations achieved by Infrared Astronomical Satellite (IRAS), Infrared Space Observatory (ISO) and the Submillimeter Common-User Bolometric Array (SCUBA), the mid-infrared (MIR) and far-infrared (FIR) observations do not reach a level of optical and near-infrared (NIR) bands, which can be explained by direct stellar emission (Hause & Dwek 2001). Stecker et al. (1992) proposed that one can use the photon attenuation in blazars to determine

[1] YITP, Kyoto University, Kyoto, Oiwake-cho, Kitashirakawa, Sakyo-ku, Kyoto, 606-8502, Japan
[2] Division of Theoretical Astronomy, NAOJ, Osawa 2-21-1, Mitaka, Tokyo, 181-8588, Japan
[3] KIPAC. Stanford University, P.O. Box 20450, MS 29, Stanford, CA, 94309, USA

the intensity of the CIB, if we know the intrinsic spectra of blazars. Subsequent studies used observations of TeV emission from blazars (for one of the latest examples, Aharonian et al. (2006)). Conversely, we could obtain the information on the maximum accelerated energy, if we know the CIB accurately. Similarly to the cases of blazars, we can expect to make use of GRBs as a probe of the CIB. However, owing to the uncertainty in GRB intrinsic spectra, the depletion due to the CIB in high-energy spectra is hard to estimate.

Observationally, GeV photons have been detected from some GRBs with the EGRET detector on the Compton Gamma-Ray Observatory. Especially, EGRET detected long lived GeV emission from GRB 940217 (Hurley et al. 1994) and GRB 930131 (Sommer et al. 1994). Although we do not know the highest energy in GRB spectra, such an existence of GeV photons makes us expect TeV photons from GRBs. Furthermore, the tentative detection of an excess of TeV photons from GRB 970417a at the $3\,\sigma$ level has been claimed with a chance probability $\sim 1.5 \times 10^{-3}$ by the water Čherenkov detector Milagrito (Atkins et al. 2000). Another possible TeV detection of GRB 971110 has been reported with the GRAND array at the 2.7σ level (Poirier et al. 2003). Staking of data from the TIBET array for a large number of GRB time window has led to an estimate of a $\sim 7\sigma$ composite detection significance (Amenomori et al. 2001). Although the statics of high energy photons are not sufficient, further observations of such very high energy gamma-ray signals by current detectors such as MILAGRO as well as MAGIC (Mirzoyan et al. 2005), VERITAS (Holder et al. 2006), HESS and CANGAROOIII (Ong 2006) might enable us to detect the signals in the near future. However, the photon detection in the TeV range can be expected only for nearby events, since high energy gamma-rays will suffer from attenuation by the CIB. On the other hand, $\sim$ GeV gamma-rays have larger mean free path against pair production. Therefore, future detectors such as Gamma-Ray Large Area Space Telescope (GLAST) will detect many GRBs and enable us to discuss such high energy gamma-ray emission from GRBs further. As noted before, primary photons are attenuated by the CIB and secondary delayed photons are produced via IC up-scattering, if GRBs emit primary TeV photons. Such delayed photons will typically have $\gtrsim$ GeV energies, which also could be detected by future detectors.

In this paper, we study the delayed spectra from GRBs most quantitatively by numerical simulations as well as an approximate formula. We focus on the effect of the CIB by including the contribution from up-scattered CIB photons (hereafter, USIB photons) to delayed secondary spectra, which has been neglected in previous works. Such a study would be important for GRBs that can emit $\sim$ TeV emission in order to know the intrinsic feature of the source. In addition, it would be useful to obtain information on the CIB more quantitatively. Not only GLAST but also MAGIC and VERITAS may detect such secondary delayed gamma-ray signals in the near future.

In §2.1, we explain the models of intrinsic GRB spectra and we describe the delayed emission mechanism in §2.2. The CIB model we use in this paper is explained in §2.3. We show the method to estimate the diffuse gamma-ray background due to GRBs in §2.4. In §3, we show the results. Finally, our summary and discussion are described in §4.

2. THE MODEL

2.1. *Model of Intrinsic Specta*

Throughout the paper, we focus on long GRBs with typical duration $T \sim 10 - 100$ s. Widths of individual pulses vary in a wide range. Typical pulses have the duration with $\delta t \sim 0.1 - 10$ s and shortest spikes have millisecond or even submillisecond widths. The internal shock model, in which the gamma-rays arise from the internal dissipation of relativistic jets, can reproduce such wide range variability. However, the simple synchrotron model cannot explain several properties of prompt emission (see, e.g., Mészáros 2006). In this paper, we do not consider these open problems on the prompt emission mechanism. The observed photon spectrum is well approximated by a broken power-law, $dN_\gamma/dE_\gamma \propto (E_\gamma/E_\gamma^{\rm b})^{-\alpha}$ for $E_\gamma^{\rm sa} < E_\gamma < E_\gamma^{\rm b}$ and $dN_\gamma/dE_\gamma \propto (E_\gamma/E_\gamma^{\rm b})^{-\beta}$ for $E_\gamma^{\rm b} < E_\gamma < E_\gamma^{\rm max}$, where $E_\gamma^{\rm sa}$ is the synchrotron self-absorption cutoff, and $E_\gamma^{\rm max}$ is the high energy cutoff.

The high energy cutoff $E_\gamma^{\rm max}$ is determined mainly by the opacity of two-photon annihilation into an electron-positron pair. In the internal shock scenario, it is easy to see that TeV photons can escape from the subshells if the internal collision radius and/or bulk Lorentz factor are large enough (Lithwick & Sari 2001).

For sufficiently high energy ranges, gamma-rays due to electron SSC, proton synchrotron and charged-meson/muon synchrotron can contribute to the intrinsic spectra via cascade processes. The resulting spectra are complicated and the study on them is beyond scope of this paper. We will investigate not the intrinsic emission but the delayed emission in detail. The delayed emission depends on the amount of attenuated photons and would not be so sensitive to the detail of the shape of intrinsic spectra with a given $E_\gamma^{\rm max}$. Throughout the paper we adopt three models with total isotropic energy $E_{\rm iso} = 10^{53}$ ergs for calculation. Model A: a broken-power law spectrum with $\alpha = 1$ and $\beta = 2.2$, $E_\gamma^{\rm b} = 300$ keV and $E_\gamma^{\rm max} = 1$ TeV. Model B: the same as Model A but $E_\gamma^{\rm max} = 10$ TeV. Model C: a numerically calculated spectrum obtained by Asano & Inoue (2007). They perform Monte Carlo simulations including synchrotron radiation, Compton scattering, pair production, synchrotron self-absorption and particles originating from protons such as electrons, positrons, muons and pions. We adopt one of their numerical results as Model C. For details, see Asano & Inoue (2007). The parameters adopted to obtain the spectrum in Model C are energy per subshell $E_{\rm sh} = 10^{50}$ ergs, $E_\gamma^{\rm b} = 300$ keV, an internal collision radius $r = 10^{15}$ cm and a Lorentz factor $\Gamma = 100$. The magnetic energy density U_B is assumed to be $0.1U_\gamma$, where U_γ is the photon energy density in the subshell. In Fig. 1, we show the intrinsic spectra for the three models we adopt. The second peak of Model C in Fig. 1 is due to SSC. Above this peak energy, photon absorption due to pair production is crucial. The intrinsic GRB duration (defined in the local rest frame) is set to $T' = 50$ s.

2.2. *Delayed Emission*

For typical GRBs at redshift $z = 1$, most high energy photons above ~ 70 GeV produce electron-positron pairs. The produced high energy pairs cause delayed high energy photon emission by IC scattering of CMB and CIB photons. The duration of such delayed emission is determined by several effects (Razzaque et al. 2004; Ando 2004); the angular spreading, IC cooling and magnetic deflection effects. The angular
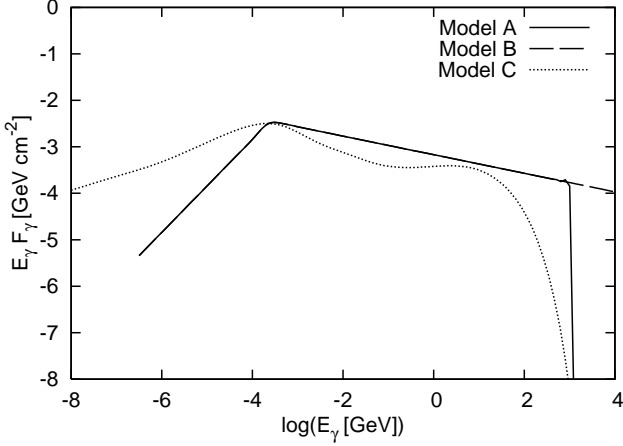
FIG. 1.— The intrinsic primary spectra we use in this paper for each model. The spectra are normalized by the fluences from a source at $z = 1$. Model parameters are described in the text.
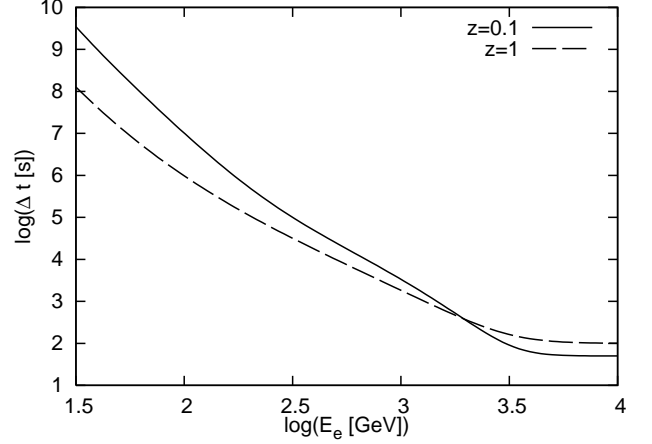

FIG. 2.— The maximum time scales for $z = 0.1$ and $z = 1$ involved in calculating the delayed secondary spectra. E_e is the electron energy in the local rest frame. The IGM field is assumed to be $B = 10^{-20}$ G.

spreading time is expressed as,

$$\Delta t_{\mathrm{ang}} \approx (1+z)\frac{\lambda_{\gamma\gamma}}{2\gamma_e^2 c} \tag{1}$$

where γ_e is the Lorentz factor of secondary electrons or positrons in the local rest frame in the Robertson-Walker metric (hereafter, the local rest frame) at each z, and $\lambda_{\gamma\gamma}$ is the photon mean free path. The IC cooling time scale is written as,

$$\Delta t_{\mathrm{IC}} \approx (1+z)\frac{\hat{t}_{\mathrm{IC}}}{2\gamma_e^2} \tag{2}$$

where $\hat{t}_{\mathrm{IC}}$ is the cooling time scale in the local rest frame. If the magnetic deflection angle is sufficiently small, the magnetic deflection time is,

$$\Delta t_B \approx (1+z)\frac{1}{2}\hat{t}_{\mathrm{IC}}\theta_B^2 \tag{3}$$

where $\theta_B = c\hat{t}_{\mathrm{IC}}/r_L$ is the magnetic deflection angle and r_L is the Larmor radius of electrons or positrons. Note that we have implicitly assumed $1/\gamma_e, \theta_B \ll \theta_j$ where θ_j is opening angle of GRB jet. Taking into account the GRB duration T, the (secondary) duration time scale is estimated by the maximum time scale, $\Delta t = \max[\Delta t_{\mathrm{ang}}, \Delta t_{\mathrm{IC}}, \Delta t_B, T]$. Examples of Δt adopting the CIB model of Kneiske et al. (2004, see section 2.3) are shown in Fig. 2. In cases with a weak magnetic field such as $B \lesssim 10^{-(18-19)}$ G, the angular spreading time scale is the most important. Of course, we should note that we treat the averaged flux over the duration time scale.

The IGM field make the situation complicated and more careful treatment would be needed to evaluate the accurate time dependent flux of the delayed emission. The delayed spectra can also be the probe of the IGM field (Plaga 1995), but we do not focus on this topic in this paper and we use an IGM field with $B = 10^{-20}$ G, in which Δt_B is not so important.

We can obtain the delayed spectra from a burst with the source redshift z by an analytic approximate formula, which is given by (Blumenthal & Gould 1970; Ando 2004),

$$\frac{dF_\gamma}{dt dE_\gamma}(E_\gamma, t, z) = \int_0^t dt_p \int d\varepsilon \int_{\gamma_e^{\min}}^{\gamma_e^{\max}} d\gamma_e \left(\frac{dF_e}{dt_p d\gamma_e}\right)$$
$$\times \left(\frac{dN_\gamma}{dE_\gamma d\varepsilon d\hat{t}_d}\right) e^{-\tau_{\gamma\gamma}^{\mathrm{bkg}}(E_\gamma, z)} \hat{t}_{\mathrm{IC}} \frac{e^{-(t_d/\Delta t)}}{\Delta t}, \tag{4}$$

where the electron injection spectrum

$$\frac{dF_e}{dt_p d\gamma_e}(E_e, t_p, z) = 2\frac{dE_{\gamma,i}}{d\gamma_e}\frac{dF_{\gamma,i}}{dE_{\gamma,i}dt_p}(E_{\gamma,i}, t_p, z)$$
$$\times (1 - e^{-\tau_{\gamma\gamma}^{\mathrm{bkg}}(E_{\gamma,i}, z)}), \tag{5}$$

and the photon emission spectrum per unit time due to IC scattering

$$\frac{dN_\gamma}{dxd\varepsilon d\hat{t}_d} = \frac{2\pi r_0^2 m_e c^3}{\gamma_e}\frac{1}{\varepsilon}\frac{dn}{d\varepsilon}(\varepsilon, z)\Big[2y\ln(2y)$$
$$+ (1+2y)(1-y) + \frac{(wy)^2}{2(1+wy)}(1-y)\Big],$$
$$x \equiv \frac{E_\gamma(1+z)}{\gamma_e m_e c^2},$$
$$y \equiv \frac{xm_e c^2}{4\varepsilon\gamma_e(1-x)},$$
$$w \equiv \frac{4\varepsilon\gamma_e}{m_e c^2}. \tag{6}$$

Here, $dF_{\gamma,i}/dE_{\gamma,i}dt_p$ is the intrinsic gamma-ray spectrum from GRB prompt emission, $E_{\gamma,i} = 2\gamma_e m_e c^2/(1+z)$ is energy of primary photons (where the source redshift is taken into account), $dn/d\varepsilon$ is the photon density spectrum of the CMB and CIB in the local rest frame, and r_0 is the classical electron radius. The value t is the given observation time of the delayed emission, t_p is the time when primary photons are released, T is the GRB duration, t_d is defined by $t_d = t - t_p$ and $\tau_{\gamma\gamma}^{\mathrm{bkg}}(E_\gamma, z)$ is the optical depth for gamma-rays propagating the universe. The upper bound of the integration over γ_e is determined by the maximum energy of the primary prompt emission, i.e. $\gamma_e^{\max} = (1+z)E_\gamma^{\max}/2$. On the other hand, the lower bound of the integration over γ_e is $\gamma_e^{\min} = \max[m_e c^2/2\varepsilon, ((1+z)E_\gamma/\varepsilon)^{1/2}/2]$. We exploit Eq. (4) iteratively by substituting $(dF_\gamma/dtdE_\gamma)(\exp(\tau_{\gamma\gamma}^{\mathrm{bkg}})-1)$ into $dF_{\gamma,i}/dt_p dE_{\gamma,i}$ instead of using the intrinsic primary flux. We perform such an iterative method in order to include the IC scattering by generated pairs due to re-absorbed secondary photons.

In the above formula, it is assumed that secondary pairs are produced only at the source redshift and cooling time

scales are evaluated with quantities at the source redshift. The photon emission spectrum is evaluated with the initial energy of secondary pairs and assumed to be constant during the pairs cool. However, pairs are produced at various redshifts and the cooling rate becomes lower as they cool. Therefore, we also execute numerical simulations including IC scattering and pair creation. Based on the pair creation rate at each redshift due to the CIB (partially CMB), we follow the time evolution of the distribution functions of the primary photon $f_\gamma(E_{\gamma,i})$, secondary pairs $f_e(\gamma_e)$, and secondary photons $f_2(E_\gamma)$ from the burst time to the present time. The minimal time (redshift) step for $f_\gamma(E_{\gamma,i})$ in our simulation is $dz = 0.005$. The pair cooling process is followed with a time step $\hat{t}_{IC}/100$ until pairs become non-relativistic. While $f_\gamma(E_{\gamma,i})$ decreases monotonically with time (or remains constant for lower energy range) by attenuation, $f_2(E_\gamma)$ does not necessarily change monotonically especially for high-redshift sources, because of re-absorption. IC photon spectra are calculated using the Klein-Nishina cross section with the Monte Carlo method used in (Asano 2005). Our method can precisely treat the re-absorption of secondary photons and the energy loss process of electron-positron pairs.

2.3. *Cosmic Infrared Background*

Gamma-ray absorption due to pair creation in cosmological scales depends on the line of sight integral of the evolving density of low energy photons in the universe. To demonstrate the effect of the CIB on the delayed spectra from GRBs, we need to exploit some model of the CIB. The CIB should be explained by a theory from the first principles, but we are far from this ultimate goal owing to poor knowledge about star formation, supernova feedback, and galaxy merging and so on. So far many models of SED of the CIB produced by stellar emission and dust re-radiation in galaxies have been constructed (Totani & Takeuchi 2002; Kneiske et al. 2002; Stecker et al. 2006). For lower redshifts, these models agree with each other basically. For higher redshifts, Stecker et al. (2006) found the larger optical depths than previously thought because of intergalactic gamma-ray absorption motivated by the recent discovery of active star formation taking place in young galaxies at high redshifts. Such model uncertainties will produce corresponding differences.

In this paper, we use the CIB model developed by Kneiske

et al. (2002,2004). They developed the evolving model of the infrared-to-ultraviolet metagalactic radiation field, based directly on observed emissivities. They specially addressed the redshift evolution of the SEDs, which are constructed from realistic stellar evolution tracks combined with detailed atmospheric models (Bruzual & Charlot 1993), and also taken into account effects of re-radiation from dusts and Polycyclic Aromatic Hydrogen molecules in the infrared. Their model parametrizes the main observational uncertainties, the redshift dependence of the cosmic star formation rate and the fraction of UV radiation released from the star forming regions. Here, we adopt the "best-fit model" of Kneiske et al. (2004), which is consistent with the data obtained from recent galaxy surveys. In Fig. 3, we show the SED of the CMB+CIB we use in this paper. For details, see Kneiske et al. (2002,2004). We also assume the ΛCDM cosmology with $\Omega_m = 0.3$, $\Omega_\Lambda = 0.7$ and $H_0 = 70\,\mathrm{km s^{-1} Mpc^{-1}}$.

Given the SEDs, we can calculate the mean free path of high energy gamma-rays for pair production or pair production rate at each redshift. Especially, using the cross section of pair creation $\sigma_{\gamma\gamma}$, the optical depth for the universe is written by,

$$\tau_{\gamma\gamma}^{\mathrm{bkg}} = \int_0^z dz \left| \frac{cdt}{dz} \right| \int d\cos\theta \frac{1-\cos\theta}{2} \int d\varepsilon \frac{dn}{d\varepsilon} \frac{d\sigma_{\gamma\gamma}}{d\cos\theta}(E_\gamma, \theta, \varepsilon)$$

(7)

For details, see Kneiske et al. (2004). For reference, we plot optical depths at $z = 0.1$ for the other models in Fig. 5. Note that the simple power-law fitting formula of Casanova et al. (2006) overestimates the optical depths in comparison with the other models above $\sim$TeV.

2.4. *Diffuse Gamma-Ray Background*

If the IGM field is strong enough ($B \gtrsim 10^{-16}$ G), it is hard to detect delayed emissions as a source connecting with GRB prompt emissions, because of large Δt_B. Therefore, such emissions may be detected as the diffuse gamma-ray background emission rather than delayed emissions. The diffuse gamma-ray emission was found to be a power-law in energy and is highly isotropic on the sky (Sreekumar et al. 1998), but it may not be consistent with a simple power-law and it is still under debate (Strong et al. 2004). The origin of diffuse gamma-ray background from extragalactic sources is also an open question. Blazar is one of the most discussed
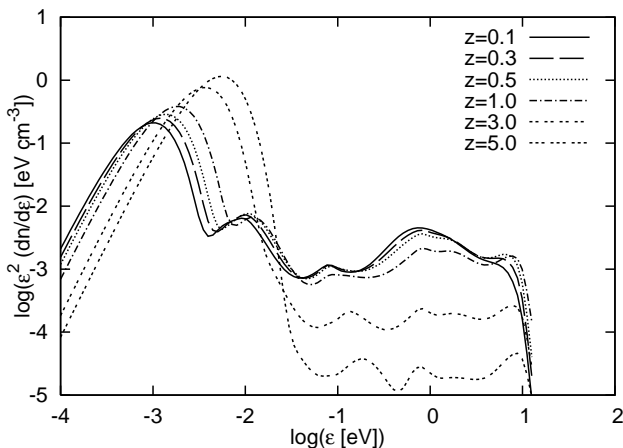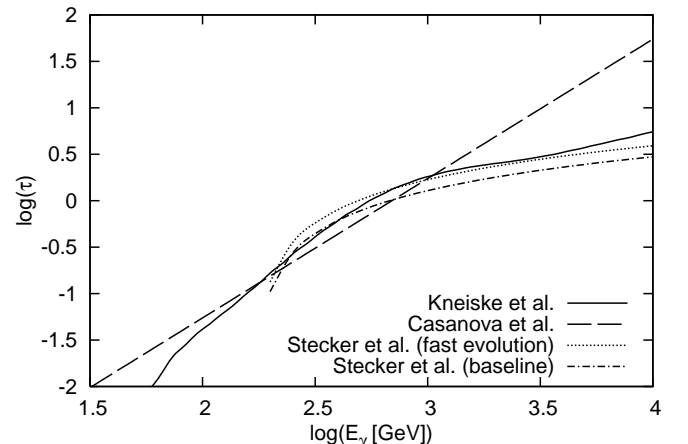

FIG. 3.— The CMB+CIB radiation field in the comoving frame for various redshifts, which we have used in this paper. The data about the CIB field are taken from the best-fit model of Kneiske et al. (2004)

FIG. 4.— The optical depth of high energy gamma-rays for $z = 0.1$.

and promising candidates. Other sources such as fossil radiation from accelerated cosmic rays during the structure formation might give a significant contribution. GRB is one of the brightest astrophysical objects and also can contribute to the gamma-ray background. GRBs as sources for the $\sim$MeV gamma-ray background was given by Hartmann et al. (2002). Casanova et al. (2006) considered GRBs as the source for $\sim$GeV-TeV gamma-ray background. However, since GRBs are rare phenomena despite of their brightness, the contribution to gamma-ray background will be small, as is shown later.

We estimate the diffuse gamma-ray background, indenpendently of the IGM, as follows. The number of GRBs is written by,

$$\dot{N}_{GRB} = \int_{z_{min}}^{z_{max}} dz \frac{\rho_{GRB}(z)}{1+z} \frac{dV}{dz}, \qquad (8)$$

where the volume factor

$$\frac{dV}{dz} = \frac{c}{H_0} \frac{4\pi d_L^2}{(1+z)^2 \sqrt{\Omega_m(1+z)^3 + \Omega_\Lambda}}, \qquad (9)$$

(d_L is the luminosity distance) and the GRB rate

$$\rho_{GRB}(z) = \rho_0 \frac{23 e^{3.4z}}{22 + e^{3.4z}} \frac{\sqrt{\Omega_m(1+z)^3 + \Omega_\Lambda}}{(1+z)^{3/2}}. \qquad (10)$$

Here, we have used SF2 model of Porciani & Madau (2001) for the GRB rate with $\rho_0 = 1\,\text{Gpc}^{-3}\text{yr}^{-1}$, assuming that the GRB rate traces the star formation rate in a global sense. Guetta et al. (2004) obtained such a value for the GRB rate and Liang et al. (2006) also reported a similar value. Even though the actual GRB rate may not be a good tracer of the star formation rate (Guetta & Piran 2007; Le & Dermer 2006), our conclusion about the diffuse background would not be changed so much because the main contribution to the background comes from bursts that occur at $z \sim (1-2)$, the number of which is observationally determined. The diffuse gamma-ray background due to GRBs is estimated by,

$$\frac{dF_\gamma}{dE_\gamma} = \int_{z_{min}}^{z_{max}} dz \left(\frac{dN_\gamma}{dE_\gamma dA}\right) \frac{d\dot{N}_{GRB}}{dz} \qquad (11)$$

where $dN_\gamma/dE_\gamma dA$ is the observed gamma-ray fluence for each burst, which is defined by,

$$\frac{dN_\gamma}{dE_\gamma dA} \equiv \frac{1}{4\pi d_p^2} \frac{dN_\gamma}{dE_\gamma}, \qquad (12)$$

where dN_γ/dE_γ is a photon number spectrum (where the source redshift is taken into account) and d_p is the proper distance to a source. We set $z_{min} = 0$ and $z_{max} = 5$.

We have to note that TeV emission from GRBs in the internal shock model can be expected only in the limited cases. In the context of the internal shock model, a sufficiently large Lorentz factor and/or large collision radius are required. Although a fraction of such GRBs that can emit TeV gamma-rays is unknown, maybe only a fraction of GRBs are TeV emitters. Hence, the contribution of GRBs to the diffuse gamma-ray background calculated in this paper, assuming that all GRBs have spectra extended to TeV energies, would give an upper limit.
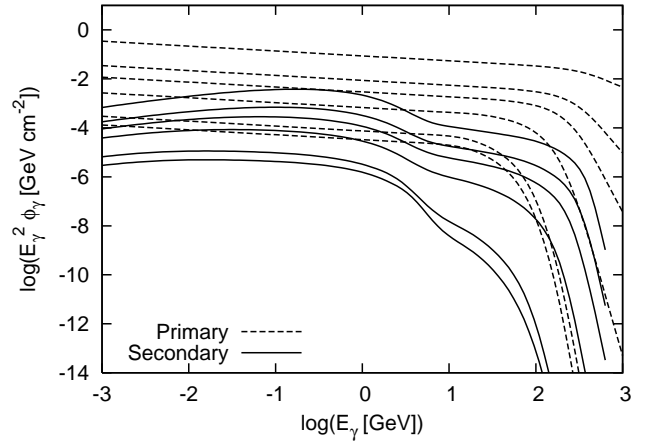
3. RESULTS

3.1. *Delayed Gamma-Ray Spectra*

FIG. 5.— The overall fluences of primary and secondary gamma-rays for model A ($E_\gamma^{max} = 1$ TeV). Redshifts (from top to bottom) are $z = 0.1$, $z = 0.3$, $z = 0.5$, $z = 1$, $z = 3$ and $z = 5$.
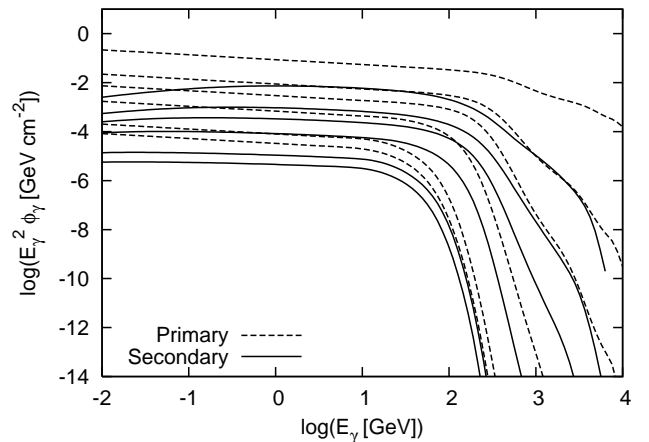

FIG. 6.— The same as Fig. 5, but for model B ($E_\gamma^{max} = 10$ TeV).

In Figs. 5 and 6, we show the total fluences of delayed emissions numerically obtained for various redshifts. In model A ($E_\gamma^{max} = 1$ TeV), the maximum energy of secondary pairs is at most ~ 500 GeV in the local rest frame. Hence, the typical energy of up-scattered CMB photons (hereafter, USMB photons) is ~ 1 GeV, above which USIB photons can give significant contributions to resulting delayed spectra. Such USIB photons show a relatively flat "slope" in spectral shape in the $\sim (10-100)$ GeV range for $z \lesssim 3$. For $z \gtrsim 3$, such high-energy slope signature becomes difficult to be seen, because secondary photons are absorbed again.

The situation changes, if E_γ^{max} is beyond 1 TeV. For model B ($E_\gamma^{max} = 10$ TeV), the maximum energy of secondary pairs is ~ 5 TeV in the local rest frame. Therefore, the energy of USMB photons can reach ~ 100 GeV. Similarly to the case of $E_\gamma^{max} = 1$ TeV, the contributions from USIB photons are important above ~ 100 GeV. However, such high energy photons may not reach the Earth, because of re-absorption. The optical depth for the high energy photons above ~ 200 GeV exceed the unity for $z \sim 0.4$. Hence, the effect of USIB photons will be buried unless GRBs occur at enough low redshifts.

Although we have discussed the CIB effects based on the fluences $E_\gamma^2 \phi_\gamma$ in Figs. 5 and 6 above, flux (F_γ) of delayed

photons rather than fluence ($E_\gamma\phi_\gamma = \int dtF_\gamma$) is often used in discussing detectability of such photons. Hence, in Fig. 7 and 8, we show fluxes that are numerically obtained for sources at $z = 0.1$. For reference, we have also plotted approximate results obtained using Eq. (4). The delayed time scale is evaluated using Eq. (1)-(3). In both Fig. 7 and 8, small difference between the numerical results and the approximate results using Eq. (4) is seen around the peak of the bump formed by USMB photons. This differences will be caused by cooled electrons. The approximation using Eq. (4) means that both the pair production and IC scattering are treated as entirely local processes. But high energy electrons will be produced after passing $\sim \lambda_{\gamma\gamma}$ and IC scattering will occur after passing $\sim \lambda_{IC} = c\hat{t}_{IC}$. These propagating electrons also suffer from IC losses as well as adiabatic losses. Hence, effective electron distribution could deviate from the expression in Eq. (5). Therefore, photon emissivity will be changed correspondingly, and the difference between two methods appears. For example, the peak of the CMB bump becomes more ambiguous due to such losses. Nevertheless, the approach using Eq. (4) will usually work as a reasonable approximation.

As is shown in Fig. 7 ($E_\gamma^{max} = 1$ TeV), delayed emissions in $\sim (10-100)$ GeV due to USIB photons are prominent. In this case, the treatment neglecting the effects of CIB photons is not good and leads to underestimating of the delayed gamma-ray flux. Even for $E_\gamma^{max} = 10$ TeV (see Fig. 8), the CIB effect is still remarkable. In fact, the contribution from CIB photons is dominant above ~ 500 GeV. However, the effect of USIB photons is smaller than the case of $E_\gamma^{max} = 1$ TeV, since a fraction of delayed secondary photons is absorbed again by CIB photons. USMB photons form the "bump" shape around the $E_\gamma \sim$ a few $\times\gamma_e^2\varepsilon_{CMB}/(1+z)$, resembling the Planck distribution. Unless the duplicated absorption of secondary photons is significant, the ratio of the fluence due to USIB photons to that due to USMB photons should reflect the ratio of the CIB energy density to the CMB density. This statement is basically demonstrated in Fig. 9, from which we can see that $E_\gamma^2\phi_\gamma$ at 100 GeV is about 0.01 times as much as that at 1 GeV for the normal CIB strength, when the burst occurs at $z = 0.1$. However, for the sufficiently high z bursts, the duplicated absorption of secondary photons becomes significant, where the fluence ratio will largely deviate from the ratio of the CIB intensity to CMB intensity. This implies that we need the delayed gamma-ray spectra over wide energy ranges in order to see the effect of USIB photons on the delayed spectra, since the cutoff of secondary emission depends on the CIB strength and the distance to the burst. Note that the number of CMB photons increases at high redshifts, while that of CIB photons does not change monotonically. Therefore, USMB photons are more remarkable for bursts at high redshifts.

In model C, the amount of prompt TeV photons is much less than that in model A, and the spectral shape is not a simple power-law. Nevertheless, the ratio of $E_\gamma^2\phi_\gamma$ in model C is close to that for model A. Thus, the 100 GeV-1 GeV ratio for low redshift bursts is a good indicator of the CIB strength irrespective of the spectral shape of prompt emissions, unless the amount of photons above TeV is considerable.

In Fig. 10 and 11, we show the time- and energy-integrated fluences above E_γ at a given time for the model A from a source at $z = 0.1$ and $z = 1$, respectively. In both figures, we change the overall CIB intensity by a factor 5 and 0.2 in order to demonstrate the effect of the CIB intensity. As we change the strength of the CIB field, the delayed secondary fluence
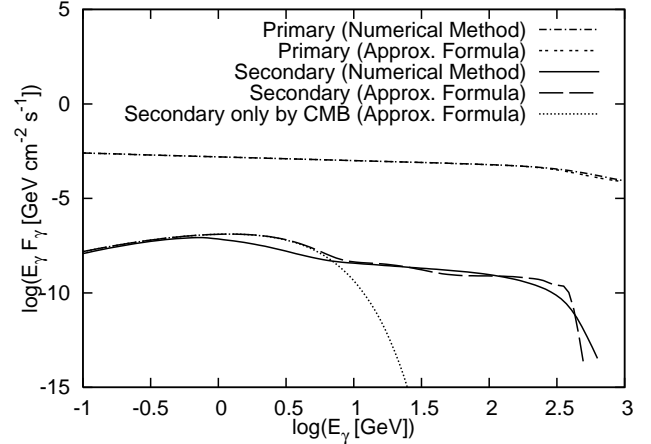

FIG. 7.— Flux for model A ($E_\gamma^{max} = 1$ TeV) obtained numerically and obtained using Eq. (4). The redshift of a source is set to $z = 0.1$. The primary flux is evaluated for the intrinsic GRB duration $T' = 50$ s (i.e. time-averaged flux over the duration is assumed). On the other hand, the delayed secondary flux is evaluated at the observation time $t = 10^4$ s (i.e. the flux which is essentially time-averaged over $t = 10^4$ s is assumed).
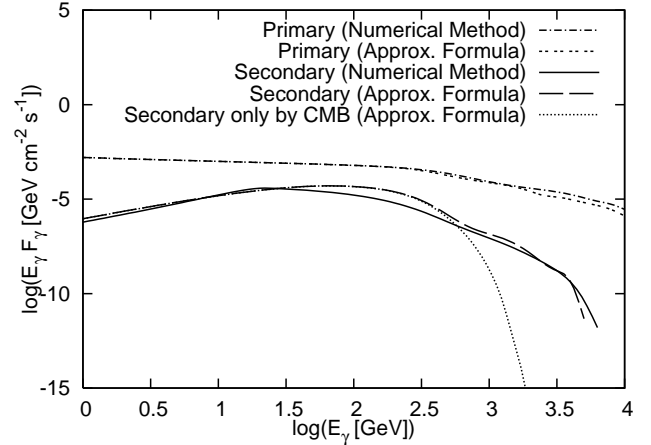

FIG. 8.— The same as Fig. 8, but for model B and the observation time $t = 10^2$ s.

also changes correspondingly, which is also shown in Fig. 9. For $z = 0.1$, the cosmic space is essentially optically thin to pair production against the CIB, so that secondary gamma-rays are not completely absorbed. The USIB effect is outstanding above $\sim (10-100)$ GeV range. Even around the bump, where USMB photons are dominant, the height of the fluence changes according to the amount of absorbed primary photons, which reflects the CIB intensity. There is also the influence on the high energy delayed spectra by duplicated absorption, but it is small for this case $E_\gamma^{max} = 1$ TeV and $z = 0.1$.

For $z = 1$, the delayed secondary spectra become more complicated. Above ~ 70 GeV, gamma-rays cannot reach the Earth without attenuation. Hence, the secondary gamma-rays above this energy are absorbed again and regenerated. If we change strength of the CIB field (as represented in the dotted or dashed line in Fig. 10 and 11), the cutoff energy, at which the optical depth becomes $\tau_{\gamma\gamma}^{bkg} = 1$, also changes. Although the strength of delayed components by USMB photons is also affected by the CIB intensity, this influence will be saturated when the primary gamma-rays are completely attenuated, for
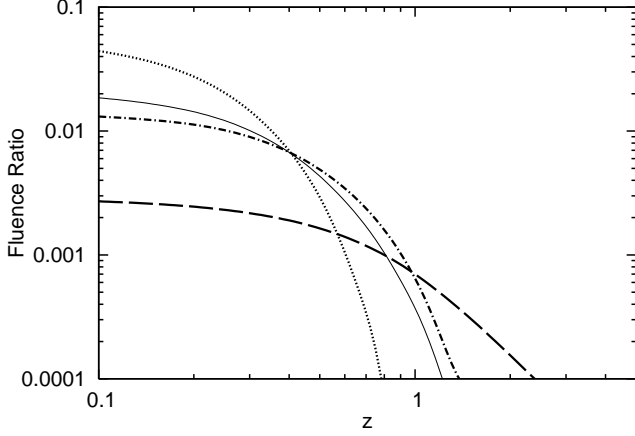
FIG. 9.— The ratio of $E_\gamma^2 \phi_\gamma$ at 100 GeV to that at 1 GeV. The thick dot-dashed line shows the energy fluence ratios for model A and the thin solid line shows those for model C in the normal CIB case, where the best-fit model given by Kneiske et al. (2004) is used. The dashed and dotted lines show the ratios for model A in the stronger CIB case (5 times as strong as the normal case) and weaker CIB case (0.2 times), respectively.
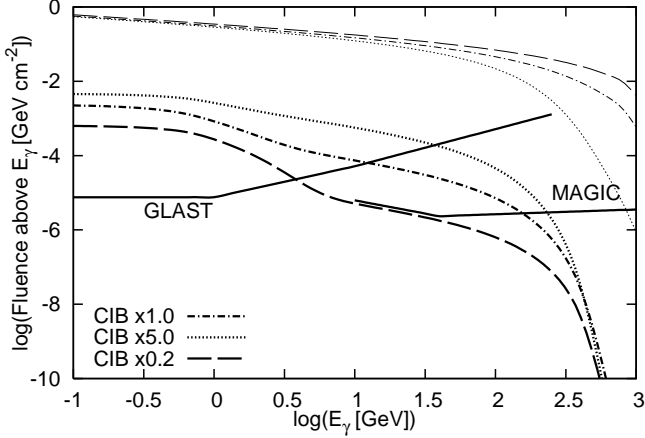

FIG. 10.— The energy-integrated fluences above a given energy E_γ. Model A with the redshift $z = 0.1$ is used. Fluences of prompt primary (upper three thin lines) and delayed secondary emission (lower three thick lines) are time-integrated over $T' = 50$ s and $t = 10^4$ s, respectively. The CIB strength is assumed to be normal (the best-fit model, dot-dashed), stronger (5 times, dotted), and weaker (0.2 times, dashed). The sensitivity curves are shown for comparison (Petry et al. 1999).

example, in the case shown in Fig. 11.

Fig. 12 and 13 show the contrastive results among the three models. For low redshift bursts as shown in Fig. 12, the high-energy slope feature is produced by the CIB for all the models. For high redshift bursts, such a high-energy slope appears for model A and model C, which is shown in Fig. 13. For model C, although a bump signature formed by USMB photons is difficult to be seen, USIB photons is still important and the delayed secondary photons above ~ 5 GeV are arising from such USIB photons. On the contrary, in the case of model B, USIB photons are almost completely absorbed again. Hence, the contribution of USIB is negligible and it is sufficient to consider USMB photons only in such a case.

In Fig. 10-13, we have also shown the sensitivity curves of GLAST and MAGIC. For 10^{53} erg bursts at $z = 0.1$, the CIB effect around $(10 - 100)$ GeV in delayed emissions could be detected by MAGIC. In addition, GLAST can also detect
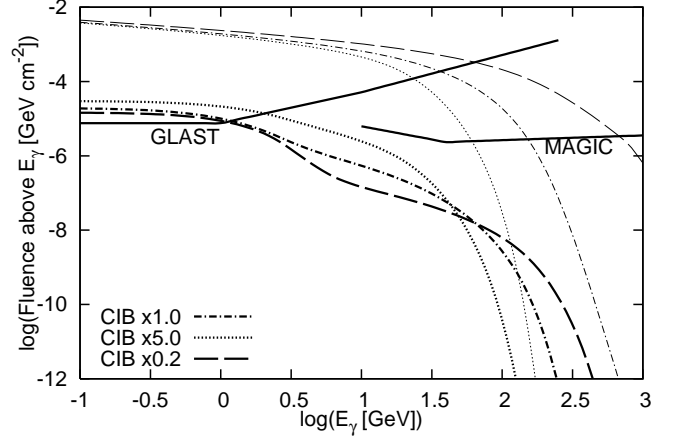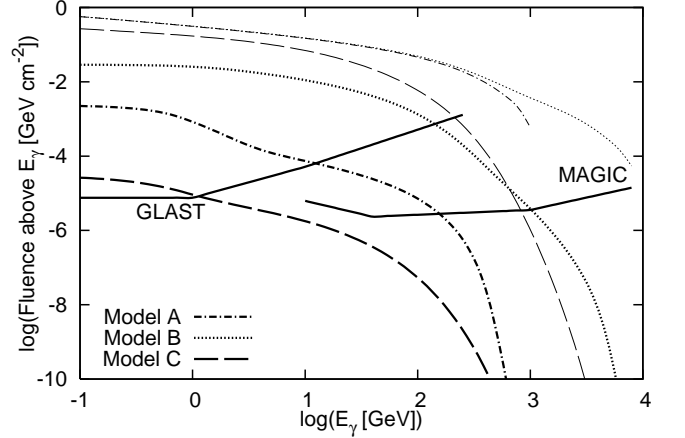

FIG. 11.— The same as Fig. 10, but for $z = 1$.

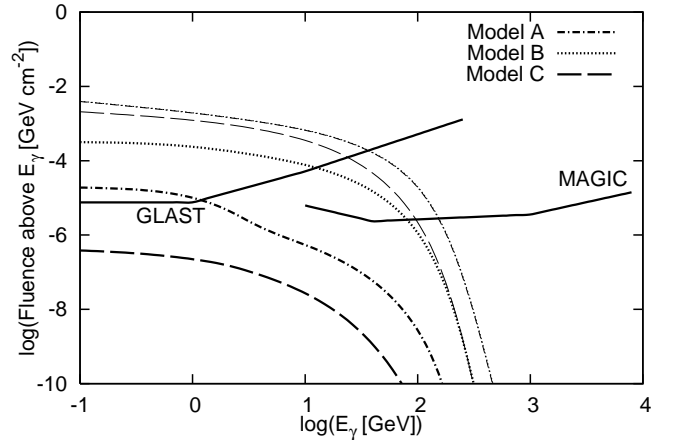FIG. 12.— The same as Fig. 10, but for models A, B and C with normal CIB strength.

FIG. 13.— The same as Fig. 12, but for $z = 1$. The dot-dashed and dotted lines are degenerate for prompt primary spectra.

$\sim (1 - 10)$ GeV delayed gamma-rays even for model C.

Even for the case of $z = 1$, MAGIC and GLAST have possibilities to detect the prompt primary signals (although MAGIC have not observed such high energy emission up to now), if GRBs of 10^{53} erg are $\sim$ 10 GeV - 10 TeV emitters.
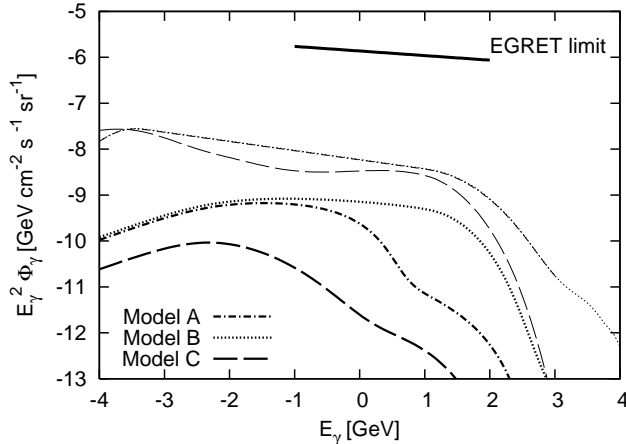
FIG. 14.— A possible diffuse gamma-ray background from GRBs for each model. It is assumed that the GRB rate traces the SF2 model with the local rate $\rho_{GRB} = 1\,Gpc^{-3}yr^{-1}$. Note that the contribution from delayed secondary emission is expected to be smaller than that from prompt primary one. The dot-dashed and dotted lines are degenerate for prompt primary spectra.

In addition, GLAST could see not only the primary component but also the secondary component, although the situation would depend on the amount of prompt TeV photons (compare model A with model C). Of course, the actual sensitivity depends on various conditions such as the direction of signals. To obtain the detectability precisely, the detailed analysis is needed with consideration about various conditions. We show the 60 s detectability in those figures for comparison with the results of spectra, but the actual sensitivity should be changed for larger observation time scales. For example, in GLAST, the fluence threshold is roughly proportional to $(t/10^5\,s)^{1/2}$ for a long integration time regime (exposure time $t \gtrsim 10^5\,s$), and is roughly constant for a short integration time regime (exposure time $t \lesssim 10^5\,s$).

3.2. *Diffuse Gamma-Ray Background*

Fig. 14 shows the resulting diffuse background in the sense of cumulative gamma-ray background. Even if the primary photons are assumed to contribute to the diffuse background, the contribution is much smaller than the EGRET limit. The contribution due to delayed emissions is much less important. This is easily understood as follows. If we assume the local GRB rate ρ_{GRB} (without beaming correction) $\sim 1\,Gpc^{-3}yr^{-1}$ and the released isotropic energy $E_{iso} \sim 10^{53}$ ergs, the Hubble time t_H ($\sim 10^{10}$ yr) and the possible cosmological evolution factor on the rate leads to the diffuse background $E_\gamma^2 \Phi_\gamma \sim (1/4\pi)cE_{iso}\rho_{GRB}(z=1)t_H \sim 10^{-7}\,GeVcm^{-2}s^{-1}sr^{-1}$, which is much smaller than the EGRET limit $\sim 10^{-6}\,GeVcm^{-2}s^{-1}sr^{-1}$ at GeV. Hence, the contribution from GRBs to gamma-ray background is expected to be at most $\sim 10\%$.

4. SUMMARY AND DISCUSSION

In this paper, we have studied the delayed secondary emission in detail under the assumption that the IGM field is sufficiently weak. We have performed the most detailed calculation to evaluate delayed GRB spectra by numerical simulations, which enable us to treat the cascade process including the multiple pair productions and IC scattering. We have also calculated the delayed spectra using Eq. (4) and compare both

results. As seen in the previous section, both methods agree with each other basically.

We have especially focused on the effect of the CIB. CIB photons play a role on not only for absorbing the high energy gamma-rays but also for being up-scattered as seed photons by created high energy pairs. USIB photons have larger energy than USMB photons, so that USIB photons are more subject to the duplicated absorption by CIB photons. The USIB component is more sensitive to the CIB than the USMB component. One of the most frequently discussing method to probe the CIB is measuring the depletion due to the CIB in prompt GRB spectra. However, owing to the uncertainty in GRB intrinsic spectra, the depletion is hard to estimate. On the other hand, an USIB signature could be more useful to probe the CIB almost irrespective of intrinsic GRB spectra as shown in Fig. 9 for models A and C.

While similar discussion can be applied to blazars (Aharonian et al. 1994; Dai & Lu 2002a), the detection of USMB and USIB photons from GRBs is also promising. As shown in Fig. 10-13, not only GLAST but MAGIC and VERITAS could detect such high energy gamma-rays arising from USIB photons for low redshift bursts. There are several characteristic features related to USIB photons: (1) The USIB signature such as a high-energy slope appears for the sufficiently low intrinsic maximum energy E_γ^{max}, and for enough low redshift bursts. (2) If (1) is satisfied (which means the duplicated absorption can be neglected), the ratio of the USIB components to the USMB components basically reflects the ratio of the CIB energy intensity to the CMB energy density. (3) The cutoff of delayed spectra is sensitive to the CIB field, because secondary photons can also be absorbed by CIB photons again. Therefore, the energy range, in which USIB photons are prominent, becomes narrower, as the redshift of the source becomes higher. (4) As long as the effective E_γ^{max} is smaller than TeV, the shape of delayed secondary spectra, especially the 100 GeV-GeV ratio, is not so sensitive to the shape of prompt primary spectra. For example, the high-energy slopes by USIB photons can be found in both model A and model C as seen in the previous section.

It is important to know the highest energy of gamma-rays. These gamma-rays, which may arise from electron synchrotron radiation, electron SSC, proton synchrotron and particles generated by photomeson or photopair production, will suffer from absorption due to electron-positron pair production. The numerical simulations in Asano & Inoue (2007) show that the maximum energy detemined by photon absorption is approximated as

$$E_\gamma^{max} \approx 10^9 \left(\frac{\Gamma}{100}\right)^4 \left(\frac{E_{sh}}{10^{51}erg}\right)^{-0.5} \left(\frac{\delta t}{1s}\right)^{1.3} eV, \quad (13)$$

where δt is the variability timescale in prompt emission. Hence, it is possible to constrain the bulk Lorentz factor by observing the highest gamma-ray energy. However, the highest gamma-ray energy can be seen in the prompt spectrum only if the attenuation due to the CIB is not significant. Because the secondary delayed emission is also influenced by highest gamma-ray energies (for example, the typical energy of the USMB bump is affected by the maximum energy E_γ^{max}), the observation of these delayed signals could provide us useful information on the source.

Now, MAGIC has continued observations and gave the upper limits for some events (MAGIC Collaboration 2006a; MAGIC Collaboration 2006b). Upper limits are also set by other detectors such as Whipple (Connaughton et al. 1997)

and STACEE (Jarvis et al. 2005). So far, no excess event above ~ 100 GeV was detected, neither during the prompt emission phase nor during the early afterglow. The upper limits between 85 and 1000 GeV are derived and compatible with a naive extension of the power-law spectra.

As we have discussed, the CIB signature in delayed spectra can be found for relatively low redshift bursts and/or GRBs with the relatively low maximum photon energy. For example, the rate of GRBs within $z = 0.2 - 0.3$ is $\sim$ a few yr^{-1}, so that we could see such delayed signals by detectors such as MAGIC in the near future. However, the event rate would be not so large. The various conditions such as a field of view and observational conditions of the detector will reduce the expected event rate significantly. Furthermore, the real rate may be smaller because a number of bursts that can emit such high energy gamma-rays may be limited. GLAST will see significant number of high energy gamma-ray emitting bursts and provide us information on high energy spectra of prompt primary spectra. In addition, by using GLAST as the monitor of GRBs that emit high energy gamma-rays, opportunities to observe high energy gamma-rays by ground telescopes will also be increased. Since GLAST may see many bursts, some of which may include ones with the delayed $\sim$ GeV components. Furthermore, the MAGICII is now being constructed and VERITAS has started observations. These advances in detectors could enable us to expect more and more chances to high energy gamma-ray signals from GRBs.

Here, we discuss possible complications. One is possible influence of environments around GRBs. We have neglected effects of the environments around host galaxies. But, there might be influences from environments such as magnetic field of the host galaxies. The second is the existence of the IGM field. In this paper, we have assumed the weak IGM field with $B \lesssim 10^{-(18-19)}$ G to estimate flux, where the magnetic deflection time is not a dominant time scale and the angular-size spreading of delayed gamma-rays is sufficiently small. Although such magnetic field might be possible in the void region, it becomes difficult to observe the delayed signals when the IGM field is strong enough. This is also the reason why the orphan delayed emission (which can be expected when $\theta_B \gtrsim \theta_j$) is difficult to be detected. Especially for $B \gtrsim 10^{-16}$ G, the delayed photons will be observed as isotropic diffuse signals that are difficult to be observed.

The third possible complication would arise from prolonged intrinsic high energy emission. TeV signals are also expected in the context of afterglow theory. Although the discrimination might be difficult, time-dependent observations could enable us to distinguish between two signals, because the time evolution will be different between the prompt emission and afterglow emission. Other possible late activities discovered by Swift would make further contamination. For example, flares can be accompanied not only by neutrinos and gamma-rays associated with the flare itself (Murase & Nagataki 2006b) but also with gamma-rays upscattered by forward shock electrons (Wang et al. 2006).

Finally, we shall comment on high energy emission from low luminosity (LL) GRBs. The recent discovery of XRF 060218 (Campana et al. 2006) implies that there may be a different population from usual cosmological high luminosity (HL) GRBs. These LL GRBs are more frequent than usual HL GRBs. If true, high energy neutrino background from LL GRBs can be comparable with that from HL GRBs (Murase et al. 2006; Gupta & Zhang 2007). Similarly, we can expect gamma-ray background from LL GRBs is comparable with that from HL GRBs. This is also pointed out by Casanova et al. (2006) and Dermer (2006). However, the diffuse gamma-ray background from GRBs is much smaller than the EGRET bound and the diffuse component will be very difficult to be detected. Furthermore, it might be difficult to emit TeV photons from LL GRBs, unless they have large Lorentz factors. Although we cannot deny the possibility for LL GRBs to emit TeV photons so far, we do not consider such cases in this paper.

REFERENCES

Aharonian, F.A. et al. 1994, ApJ, 423, L5
Aharonian, F.A. et al. 2006, Nature, 440, 1018
Amenomori, M. et al. 2001, AIPC. Proc., 599, 493
Ando, S. 2004, MNRAS, 354, 414
Asano K. 2005, ApJ, 623, 67
Asano, K., and Inoue, S. 2007., in preparation
Asano, K., and Nagataki, S. 2006, ApJ, 640, L9
Asano, K., and Takahara, F. 2003, PASJ, 55, 433
Atkins, R. 2000, ApJ, 533, L119
Blumenthal, G.R., and Gould, R.J. 1970, Rev. Mod. Phys., 42, 237
Bruzual, A. G., and Charlot, S. 1993, ApJ, 405, 538
Campana, et al. 2006, Nature, 442, 1008
Casanova, S., Dingus, B., and Zhang, B. 2006, Gamma-Ray Bursts in the Swift Era (Washington, DC) Edited by Holt, S., Gehrels, N., and Nousek, J.A., AIPC. Proc., 836, 113 (American Institute of Physics)
Cheng, L.X., and Cheng, K.S. 1996, ApJ, 459, L79
Connaughton, V. et al. 1997, ApJ, 479, 859
Dai, Z.G., and Lu, T. 2002, ApJ, 580, L7
——. 2002, ApJ, 580, 1013
Dermer, C.D. 2006, astro-ph/0610195
Dermer, C. D., & Atoyan, A. 2003, Phys. Rev. Lett., 91, 071102
Dermer, C.D., and Atoyan, A. 2004, A&A, 418, L5
Dermer, C.D., Chiang, J., and Mitman, K. 2000, ApJ, 537, 785
Derishev, E. V., Kocharovsky, V. V., and Kocharovsky, Vl. V. 2001, A&A, 372, 1071
Guetta, D., Spada, M., & Waxman, E. 2001, ApJ, 559, 101

Guetta, D., and Granot, J. 2003, ApJ, 585, 885
Guetta, D., Hooper, D., Alvarez-Muñiz, J., Halzen, F., & Reuveni, E. 2004, Astroparticle Phys., 20, 429
Guetta, D., Perna, R., Stella, L., and Vietri, M. 2004, ApJ, 615, L73
Guetta, D., and Piran, T. 2007, astro-ph/0701194
Gupta, N., and Zhang, B. 2007, Astroparticle Phys., in press
Hartmann, D.H. et al. 2002, AIPC. Proc., 662, 477G
Hause, M.G., and Dwek, E. 2001, ARA&A, 39, 249
Holder et al. 2006, astro-ph/0611598
Hurley et al., 1994, Nature, 372, 652
Jarvis, B. et al. 2005, Proc. of the 29th International Cosmic Ray Conference, 4, 455
Kneiske, T.M., Mannheim, K., and Hartmann, D.H. 2002, A&A, 386, 1
Kneiske, T.M. et al. 2004, A&A, 413, 807
Le, T., and Dermer, C.D. 2006, astro-ph/0610043
Liang, E. 2006, astro-ph/0605200
Lithwick, Y., and Sari, R. 2001, ApJ, 555, 540
MAGIC Collaboration, 2006, ApJ, 641 L9
MAGIC Collaboration, 2006, astro-ph/0612548
Mészáros, P. 2006, Rep. Prog. Phys., 69, 2259
Mészáros, P., Rees, M. J. 1994, MNRAS, 269, L41
Mészáros, P., Rees, M. J., Papathanassiou, H. 1994, ApJ, 432, 181
Mirzoyan et al. 2005, Proc. of the 29th International Cosmic Ray Conference, 4, 23
Murase, K., and Nagataki, S. 2006a, Phys. Rev. D, 73, 063002
——. 2006b, Phys. Rev. Lett., 97, 051101

Murase, K., Ioka, K., Nagataki, S., and Nakamura, T. 2006, ApJ, 651, L5
Ong, R.A. 2006, astro-ph/0605191
Papathanassiou, H., and Meszaros, P., ApJ, 471, L91
Peer, A., and Waxman, E. 2004, ApJ, 613, 448
Petry, D. et al. 1999, A&A, 138, 601
Poirier at al. 2003, Phys. Rev. D, 67
Porciani, C., and Madau, P. 2001, ApJ, 548, 522
Plaga, R. 1995, Nature, 374, 30
Razzaque, S., Mészáros, P., and Zhang, B. 2004, ApJ, 613, 1072
Sreekumar, P. et al. 1998, ApJ, 494, 523
Stecker, F.W., de Jager, O.C., and Salamon, M.H. 1992, ApJ, 390, L49
Stecker, F.W., Malkan, M.A., and Scully, S.T. 2006, ApJ, 648, 774

Sommer, M. 1994, ApJ, 422, L63
Strong, A.W., Moskalenko, I.V., and Reimer, 0. 2004, ApJ, 648, 774
Totani, T. 1998, ApJ, 509, L81
Totani, T., and Takeuchi, T.T. 2002, ApJ, 570, 470
Wang, X.Y., Dai, Z.G., and Lu, T. 2001, ApJ, 556, 1010
Wang, X.Y. et al. 2004, ApJ, 604, 306
Wang, X.Y., Li, Z., and Mészáros, P. 2006, ApJ, 604, 306
Waxman, E. and Bahcall, J. 1997, Phys. Rev. Lett., 78, 2292
Zhang, B. 2007, astro-ph/0701520
Zhang, B., and Mészáros, P. 2001, ApJ, 559, 110